Numerical Simulations of the Wake of Kauai

TODD P. LANE

School of Earth Sciences, The University of Melbourne, Melbourne, Australia, and National Center for Atmospheric Research, Boulder, Colorado*

ROBERT D. SHARMAN

National Center for Atmospheric Research, Boulder, Colorado*

ROD G. FREHLICH

National Center for Atmospheric Research, and Cooperative Institute for Research in Environmental Sciences, University of Colorado at Boulder, Boulder, Colorado*

JOHN M. BROWN

NOAA/Forecast Systems Laboratory, Boulder, Colorado

(Manuscript received 30 June 2005, in final form 26 January 2006)

ABSTRACT

This study uses a series of numerical simulations to examine the structure of the wake of the Hawaiian island of Kauai. The primary focus is on the conditions on 26 June 2003, which was the day of the demise of the Helios aircraft within Kauai's wake. The simulations show that, in an east-northeasterly trade wind flow, Kauai produces a well-defined wake that can extend 40 km downstream of the island. The wake is bounded to the north and south by regions of strong vertical and horizontal shear—that is, shear lines. These shear lines mark the edge of the wake in the horizontal plane and are aligned approximately parallel to the upstream flow direction at each respective height. The highest-resolution simulations show that these shear lines can become unstable and break down through Kelvin–Helmholtz instability. The breakdown generates turbulent eddies that are advected both downstream and into the recirculating wake flow. Turbulence statistics are estimated from the simulation using a technique that analyzes model-derived structure functions. A number of sensitivity studies are also completed to determine the influence of the upstream conditions on the structure of the wake. These simulations show that directional shear controls the tilt of the wake in the north–south plane with height. These simulations also show that at lower incident wind speeds the wake has a qualitatively similar structure but is less turbulent. At higher wind speeds, the flow regime changes, strong gravity waves are generated, and the wake is poorly defined. These results are consistent with previous idealized studies of stratified flow over isolated obstacles.

1. Introduction

An important component of topographic flows is the wake that forms in the lee of isolated islands or mountain ranges. Early satellite images identified the existence of island wakes (e.g., Hubert and Krueger 1962; Chopra and Hubert 1965), which were visible in cloud fields as unstable vortex streets. Striking examples of such wakes are now easily found within the vast quantities of high-resolution satellite imagery available today. Usually these wakes are visible in the lee of isolated islands, when the wake flow modulates stratocumulus cloud layers, highlighting vortices that can be quasi steady and attached to the island or unstable vortices that are periodically shed downstream. Island wakes can influence downstream precipitation, can de-

* The National Center for Atmospheric Research is sponsored by the National Science Foundation.

Corresponding author address: Todd Lane, School of Earth Sciences, The University of Melbourne, Melbourne, Victoria 3010, Australia.
E-mail: tplane@unimelb.edu.au

fine the prevailing wind in the lee of the island, and can produce turbulence and mixing downstream.

There is a vast body of literature concerning the structure of wakes behind isolated obstacles in stratified flows, based on both laboratory experiments (e.g., Hawthorne and Martin 1955; Brighton 1978; Hunt and Snyder 1980; Castro et al. 1983; Baines 1995) and numerical modeling studies (e.g., Smolarkiewicz and Rotunno 1989; Vosper 2000; Epifanio and Durran 2002; Hafner and Xie 2003; Epifanio and Rotunno 2005). These studies have examined the dynamics of wake formation in cases with smooth topography and have successfully described the way in which different flow regimes vary as a function of nondimensional numbers such as the Reynolds number Re ($=UL/\nu$) and nondimensional mountain height[1] $\hat{h}$ ($=Nh/U$), where U is the incident flow speed, N is the Brunt–Väisälä frequency, h is the obstacle height, L is the obstacle length, and ν is the kinematic viscosity. For example, these studies have shown that for $\hat{h} \ll 1$ the flow is in a "gravity wave" regime in which the majority of the flow is over the mountain, hence generating mountain waves with little evidence of a wake. As $\hat{h}$ is increased the flow becomes blocked and some portion of the fluid moves laterally around the mountain, contributing to the formation of a wake. Smolarkiewicz and Rotunno (1989) showed that at $\hat{h} \sim 2$ flow stagnation can occur at both the upstream and downstream sides of the mountain and the wake appears as a set of counterrotating vortices attached to the lee slope. Vosper (2000) showed that at larger nondimensional mountain heights ($\hat{h} >$ 10) these vortices can become unstable and are shed downstream.

The inclusion of complex topography and realistic atmospheric environments complicates the dynamics and structure of island wakes. There have, however, been a number of detailed experiments and case studies that examined observed island wakes. The most extensive set of studies stemmed from a number of field experiments that examined the wake of the island of Hawaii through both observations (e.g., Smith and Grubišić 1993) and numerical simulations (e.g., Smolarkiewicz et al. 1988). These studies were in the easterly trade wind regime, with flow conditions that equated to $\hat{h} \sim 2.5$–4. Both cited studies showed that Hawaii's wake consists of two large quasi-steady counterrotating vertical vortices, with the width of the wake approximately equal to the diameter of the island. Smith and Grubišić also showed that as the low-level flow passed around the island it was accelerated to form two low-level jets, one to the north and one to the south of the island. These jets helped to define the edges of the wake, which were characterized by strong horizontal gradients in wind speed, that is, shear lines, and within these shear lines there was some evidence of enhanced turbulence (see Smith and Grubišić 1993, their Fig. 8). As a consequence of the Hawaii topography, the strength of the shear zones was asymmetric, with the southern shear line being narrower and better defined than the northern shear line. Other case studies of island wakes include a detailed observational and modeling study of the wake of St. Vincent (Smith et al. 1997) and a very high resolution modeling study of turbulence generated in the wake of Lantau Island (Clark et al. 1997).

Although there have been a number of studies focusing on the island of Hawaii, the other islands in the Hawaiian chain have been somewhat overlooked. All islands in the Hawaiian archipelago exhibit downstream wakes, which often show up clearly in satellite sun-glint photographs in which the smoother sea surface in the wake with its velocity deficit is in contrast to the rougher seas in the trade wind regions outside the wake. An example is shown in Fig. 1; wakes in the lee of the islands of Kauai and Oahu are obvious. Scatterometer measurements indicate that the wake may extend considerable distances downstream, especially for the larger islands (Xie et al. 2001). The study presented here examines the near-field wake of Kauai in detail. Kauai is the westernmost large island in the Hawaiian chain, is about 40 km in diameter, and peaks at approximately 1600 m high. Kauai is roughly one-half as tall as Hawaii, and therefore, for fixed wind and stability conditions, Kauai's nondimensional mountain height will be approximately one-half as large as Hawaii's and thus may have a different wake structure.

The wake of Kauai has been examined by Burk et al. (2003) using numerical simulations, with a focus on the effects of the (relatively dry) wake on radar signal propagation. In their study, they examined the downstream extent of the wake and the wake's sensitivity to nondimensional mountain height (which was investigated by varying terrain height for fixed upstream flow conditions). As in the Hawaii investigations, they also found that the wake was bounded to the north and south by shear lines. The current study extends the results of Burk et al. (2003) by examining the structure of the near-field wake and the shear lines in more detail, with a focus on the generation of turbulence within the wake and quantitative estimates of small-scale velocity statistics.

This particular study of Kauai's wake is motivated by

[1] In many previous studies this term is referred to as the inverse Froude number (1/Fr). See Baines (1995) for a discussion of this terminology.

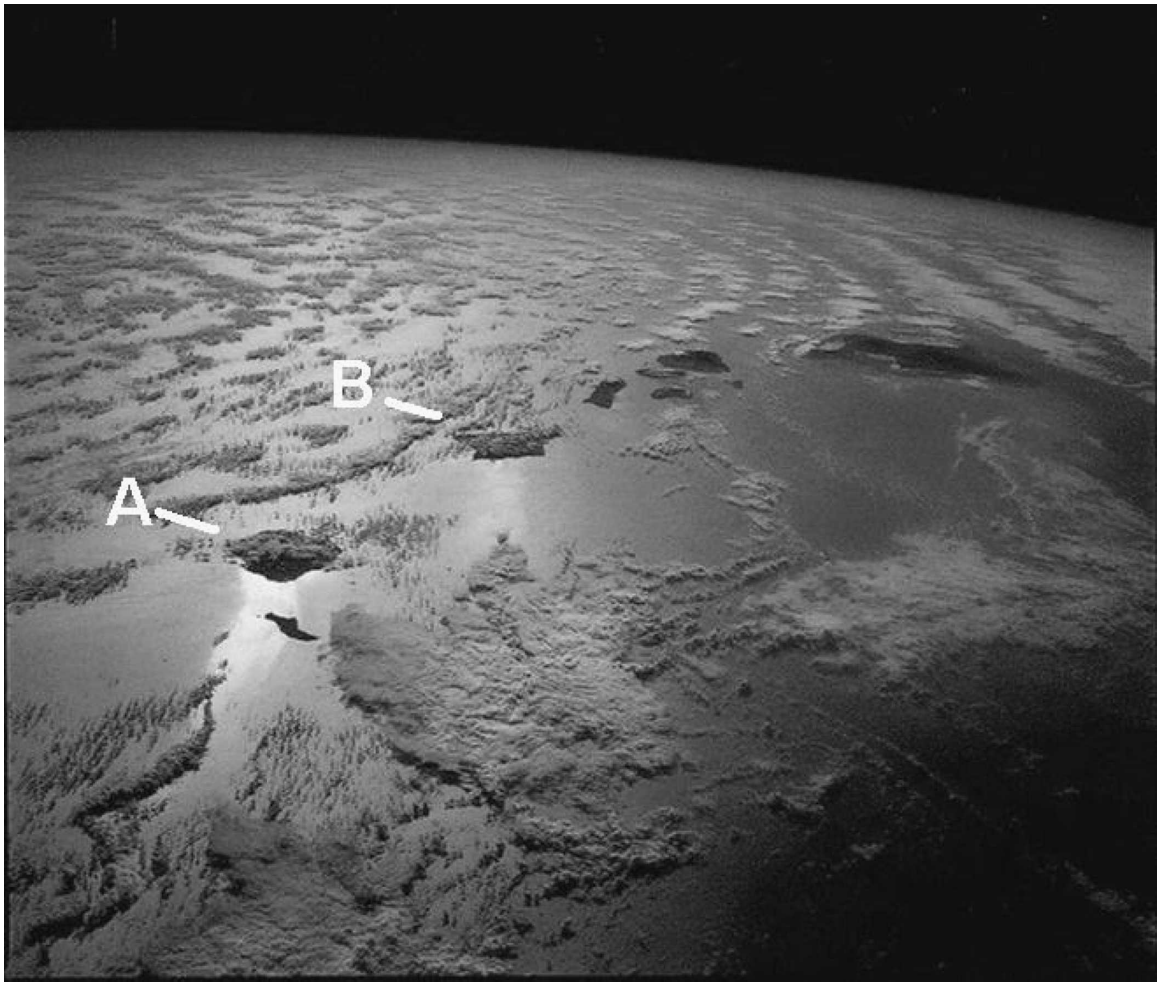

FIG. 1. Satellite image of the Hawaiian Island chain (looking toward the east). A wake is particularly evident in the sun-glint contrast downstream of Kauai (A) and, to a lesser extent, Oahu (B). The source, time, and date of the image are unknown.

the breakup of the Helios experimental aircraft. The Helios was an unmanned solar-powered aircraft that was designed for ultralong, very high altitude flight. Helios's wingspan was 247 ft (~75 m), and in 2001 it broke the world altitude record for propeller-driven flight by reaching 96 863 ft (~29 524 m) (Teets et al. 2002). Helios operated from the Pacific Missile Range Facility (PMRF) on the western side (and therefore in the wake) of Kauai. PMRF was chosen for operations because of the relatively calm winds at that location and because it is surrounded by extensive controlled airspace (Teets et al. 2002; Ehernberger et al. 2004). Shortly after takeoff on the day of interest, 26 June 2003, the Helios entered an aerodynamic stall at an altitude of about 900 m, followed by an uncontrolled steep dive, and was destroyed when it crashed into the ocean. The aircraft track from takeoff to breakup is shown in Fig. 2, highlighting the importance of the northern part of Kauai's wake and the variability of the wind within the wake. At the request of the National Aeronautics and Space Administration (NASA) Helios Mishap Review Board, we completed simulations to document the structure of the wake of Kauai, including its horizontal and vertical extent, and to estimate turbulence levels within the wake.

The aim of this study is to document the structure of the wake of Kauai on 26 June 2003 using numerical simulations and to examine the occurrence of turbulence within the wake. Sensitivity studies are completed to examine the processes controlling some of the key features of the wake, yet it is not the purpose of this study to explore the entire parameter space of Kauai's wake, but rather just those features that may be important for understanding the wake structure on 26 June 2003.

The remainder of the paper is arranged as follows.

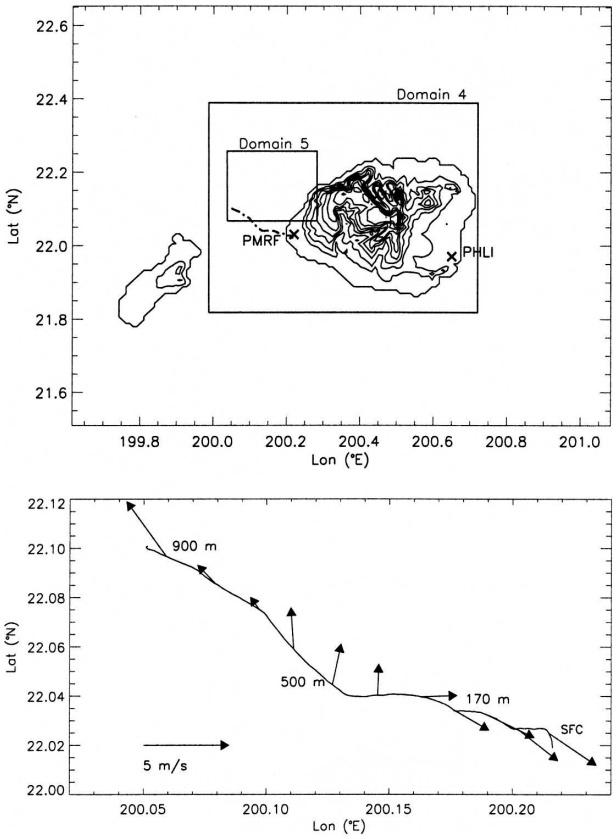

FIG. 2. (top) The numerical model's domain 3, showing the topography of Kauai and the smaller island of Niihau, contoured at 150-m intervals. The locations of domains 4 and 5, the PMRF, and Lihue (PHLI) are marked. Also shown is the flight track of the Helios on 26 Jun 2003 (dot–dashed) emanating from PMRF. (bottom) The Helios flight track, with Helios-measured horizontal wind vectors shown and relevant flight altitudes along the flight track marked.

The numerical model used and the 26 June simulations are described in section 2, including a description of the wake, its breakdown into turbulence, and a characterization of the turbulence. The sensitivity of the wake to upstream conditions is examined in section 3. The results are summarized in section 4.

2. The numerical model and simulations of 26 June 2003

a. Model outline

The numerical model that is used for this study is the same as that used by Smolarkiewicz et al. (1988) and Rasmussen et al. (1989) to study the wake in the island of Hawaii and the formation of upstream cloud bands. This model was originally developed by Clark (1977), with subsequent updates and improvements (e.g., Clark and Hall 1996). The model is a finite-difference approximation to the three-dimensional, anelastic, nonhydrostatic equations of motion. The model uses a terrain-following coordinate transform, second-order spatial and temporal advection schemes, explicit treatment of cloud processes, and a first-order subgrid-scale closure. One particular feature of the model that is utilized in the current study is its two-way interactive grid-nesting capability (Clark and Farley 1984). This capability allows the large-scale features of the flow to evolve while simulating smaller-scale features in limited areas.

TABLE 1. Summary of model domain geometry, including the number of grid points in the zonal (NX), meridional (NY), and vertical (NZ) directions; the horizontal grid spacing ($\Delta X = \Delta Y$); the vertical grid spacing above the surface layer (ΔZ); the domain depth (H); and the time step (ΔT).

Domain	NX	NY	NZ	ΔX (m)	ΔZ (m)	H (km)	ΔT (s)
1	90	90	100	6000	200	18.7	30
2	100	100	110	3000	100	9.9	20
3	152	128	100	1000	100	8.9	10
4	152	128	100	500	50	4.0	2.5
5	152	128	90	167	50	3.5	1.25

The model domain configurations are summarized in Table 1 and Fig. 2. Each interior domain takes its boundary conditions from the next-coarsest domain. The outermost domain (domain 1) uses open lateral boundaries and a Rayleigh friction absorber in the uppermost 8 km to mitigate the reflection of disturbances from the model lid. Most of the analyses presented within this paper use the first three domains only, and, unless stated otherwise, the results from the domain with 1-km grid spacing (domain 3) will be presented. Domain 3 is shown in Fig. 2; it encompasses the entire island of Kauai and resolves most of the wake structure.

The model topography is defined at the finest grid resolution, 167 m, and undergoes appropriate averaging for the coarser domains. This averaging also removes features in the topography with scales equal to 2 times the horizontal grid spacing. Surface friction is parameterized using a roughness length formulation. The roughness length is 5×10^{-4} m over the ocean and 0.5 m in regions in which the topography is higher than 1 km, and it is a linear function of topographic height between these values. The modeled wake structure was found to be insensitive to surface friction values, and a similar wake formed in a simulation with no surface friction.

All simulations to be presented are initialized using a single sounding. That is, at the initial time the modeled flow is assumed to be horizontally homogeneous with a vertical structure that is defined by a single vertical profile. This vertical profile defines the wind and ther-

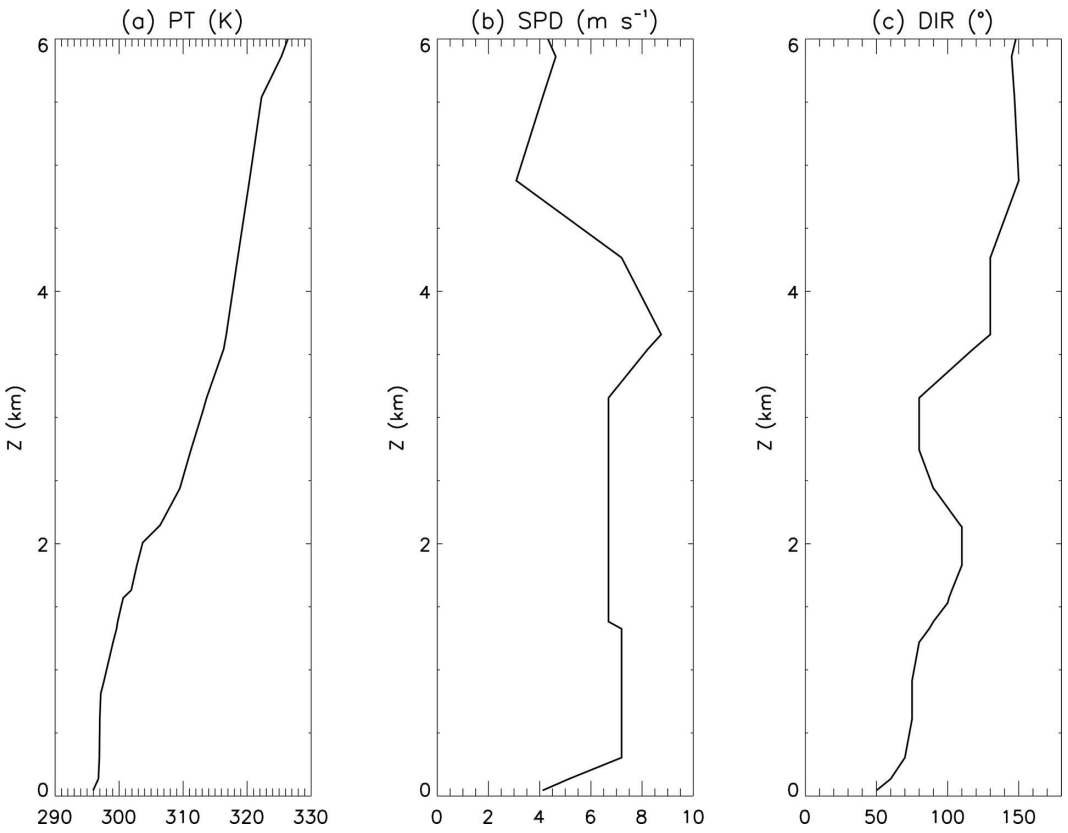

FIG. 3. Profiles of (a) potential temperature, (b) wind speed, and (c) wind direction from the 1200 UTC 26 Jun 2003 Lihue (PHLI) sounding.

modynamic variables. Each simulation is run for at least 6 h after initialization; by this time the wake has reached a quasi-steady state.

b. 26 June 2003 simulation

In this section the 26 June 2003 simulation is described. This simulation uses the 1200 UTC 26 June 2003 rawinsonde sounding that was released from Lihue (Fig. 3). The location of Lihue, marked on Fig. 2, is on the southeastern side of the island. This sounding was considered to be the best representation of the upstream flow conditions; however, it does include some influence from island-induced circulations. These influences will be discussed later in the section. The 1200 UTC sounding nominal release time corresponds to 0200 local time (LT) 26 June, which was approximately 8 h before the Helios mishap. The sounding features a trade wind inversion at about 1700 m MSL (i.e., above the mountain top), with the low-level winds from the northeast with speeds of about 7 m s^{-1}. The wind shifts to easterly near the inversion, and there is a flow reversal above 7 km.

Below 1600 m (mountain height), the sounding observed the wind speed to be approximately 7 m s^{-1} (a typical value; see Rasmussen et al. 1989) and the average Brunt–Väisälä frequency to be approximately 0.007 s^{-1}. Therefore, the nondimensional mountain height is approximately 1.67, which is somewhat smaller than in the simulations of Smolarkiewicz et al. (1988) and Rasmussen et al. (1989) ($\hat{h} \sim 2.5$–5). There is, however, some ambiguity in assigning a single value to $\hat{h}$ in flows such as this for which both the wind speed and stability vary over the depth of the mountain and the mountain height h is not well defined because of the complex topography.

Observations from PMRF suggested that the seabreeze circulation induced by the island's surface heating may influence the low-level flow within the wake [see also Leopold (1949) and Lavoie (1967)]. However, as mentioned earlier, the simulation uses a single-sounding initialization integrated in time to a quasi-steady state. Therefore, the assignment of a valid time to the simulation is arbitrary. The effect of surface heating and the sea–land heating contrast was included in the simulations by assuming that the initial time of the model was 0400 LT. The model uses solar heating and

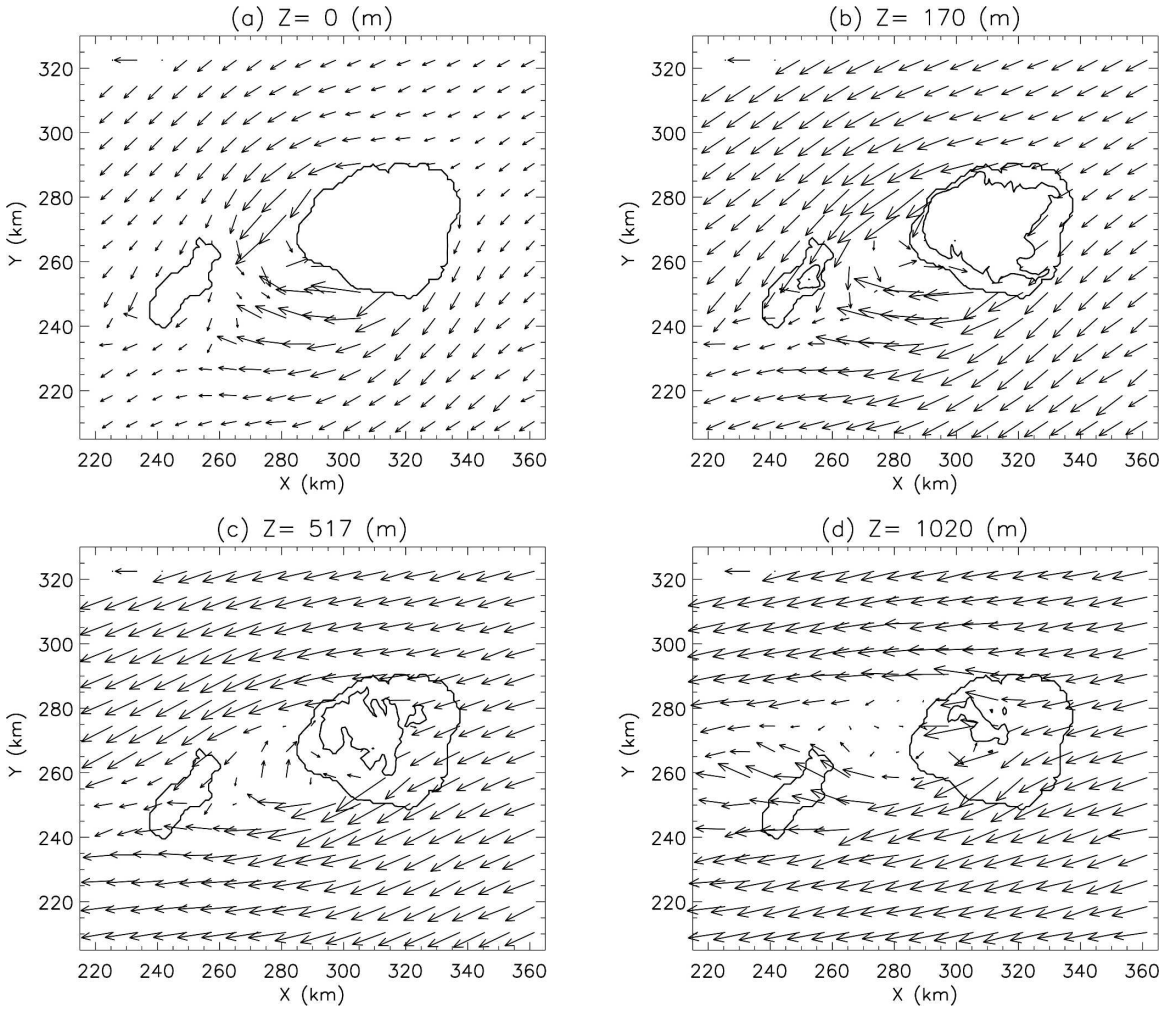

FIG. 4. Horizontal wind vectors at (a) sea level, (b) 170 m MSL, (c) 517 m MSL, and (d) 1020 m MSL from domain 3 for the simulation initialized with the 1200 UTC 26 Jun Lihue sounding. Also shown are the coastline and the topography contour that intersects the relevant altitude. The coordinate axes are relative to the southwestern corner of the outermost domain, and the vector in the upper-left corner represents 5 m s^{-1}.

topography shadowing, with the albedo over land taken to be 0.14, with zero sensible heat flux over water. The modeled sunrise is at approximately 0600 LT, and therefore 6 h of integration assigns a valid time to the simulation of 1000 LT.

Horizontal wind vectors at 0, 170, 500, and 1000 m MSL are shown in Fig. 4 at 6 h into the simulation. At sea level (Fig. 4a), the upstream northeasterly flow shows strong blocking, with wind vectors aligned approximately parallel to the coastline on the upstream side of the island. This deviated flow accelerates into the lee of the island, with two low-level jets: one easterly jet (from the south side of the island) and one northeasterly jet (from the north side of the island). Between these two jets is a relatively narrow region of slower recirculating flow, which is reversed from its upstream direction and is directed onshore, in qualitative agreement with the observations of the Hawaiian wake by Smith and Grubišić (1993). At 170 m (Fig. 4b), evidence of blocking is reduced and there is less deviation of the upstream flow around the mountain. In the lee, the two jets remain but are farther apart; that is, the width of the region of reversed flow is larger. At 500 m (Fig. 4c), the flow features a well-defined wake that extends about 30 km downstream from the western shore of Kauai. The edges of the wake are defined by a strong reduction in wind speed from approximately its background value to being almost stagnant within the wake. Within the wake, the strong onshore flow is not present and the flow features two relatively large eddies (or vertical vortices). The edges of the wake are aligned approximately with the upstream flow direction. At

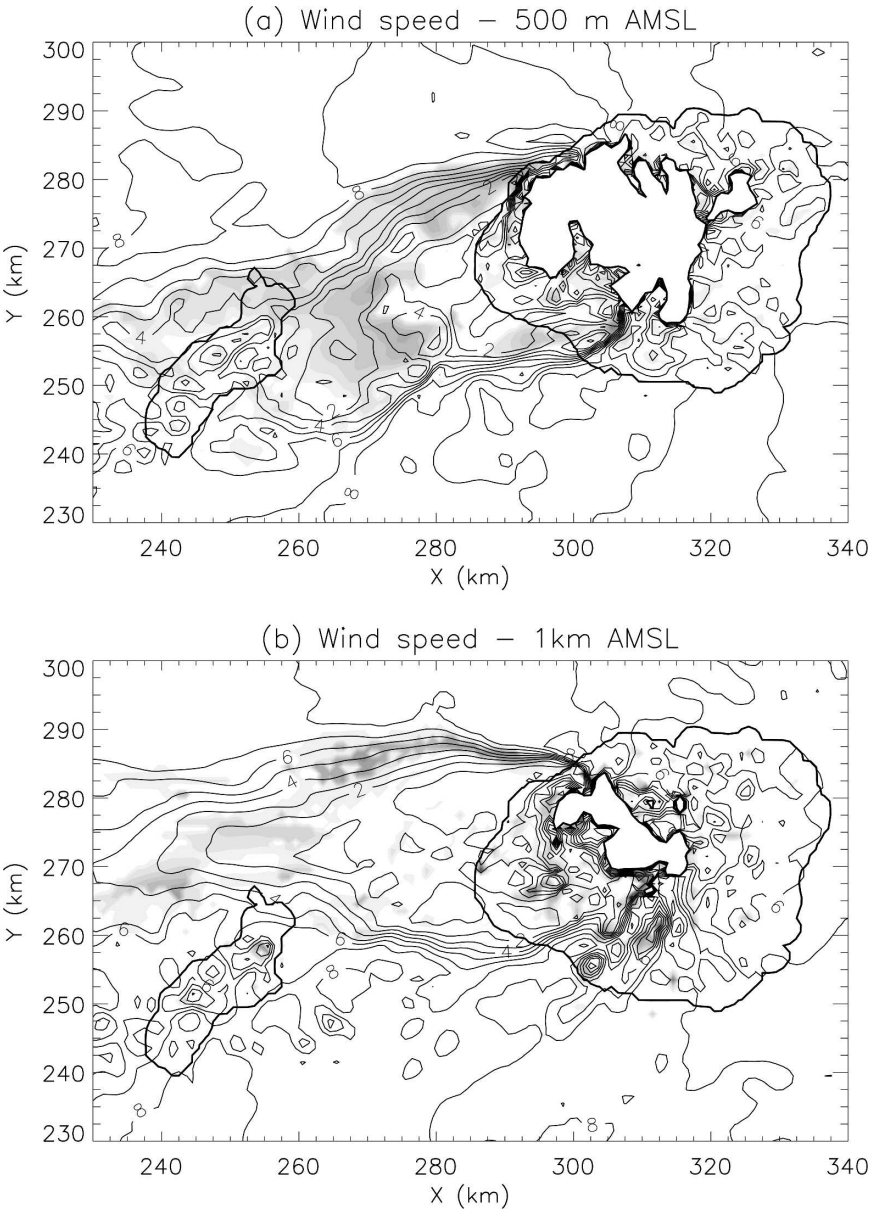

FIG. 5. Horizontal cross section of wind speed at (a) 500 and (b) 1000 m MSL from domain 3 of the 1200 UTC 26 Jun simulation. Wind speed contours have 1 m s^{-1} interval. Also shown is parameterized TKE (shaded); the maximum TKE in (a) is approximately 1 m^2 s^{-2} and in (b) is approximately 0.7 m^2 s^{-2}. Note that these figures do not show the entire horizontal extent of domain 3.

1000 m (Fig. 4d), the upstream flow has a weaker northerly component and is therefore more easterly. Likewise, the wake is aligned more east–west. At this height the wake is well defined and consists of a large region with much slower wind speed in comparison with the upstream flow. The wake extends about 40 km downstream, is quasi steady, and remains attached to the mountain.

Horizontal cross sections of wind speed (Fig. 5) show that the boundary of the wake is defined by strong horizontal shear zones, or shear lines. Outside of the wake, the flow is relatively undisturbed; within the wake, the wind is weak (~1 m s^{-1}). The orientation of the shear lines, and hence the orientation of the wake itself, compare well to the upstream flow direction. For example, at 500 m the shear lines are oriented from east-northeast to west-southwest, and at 1 km the shear lines are oriented from approximately east to west. The

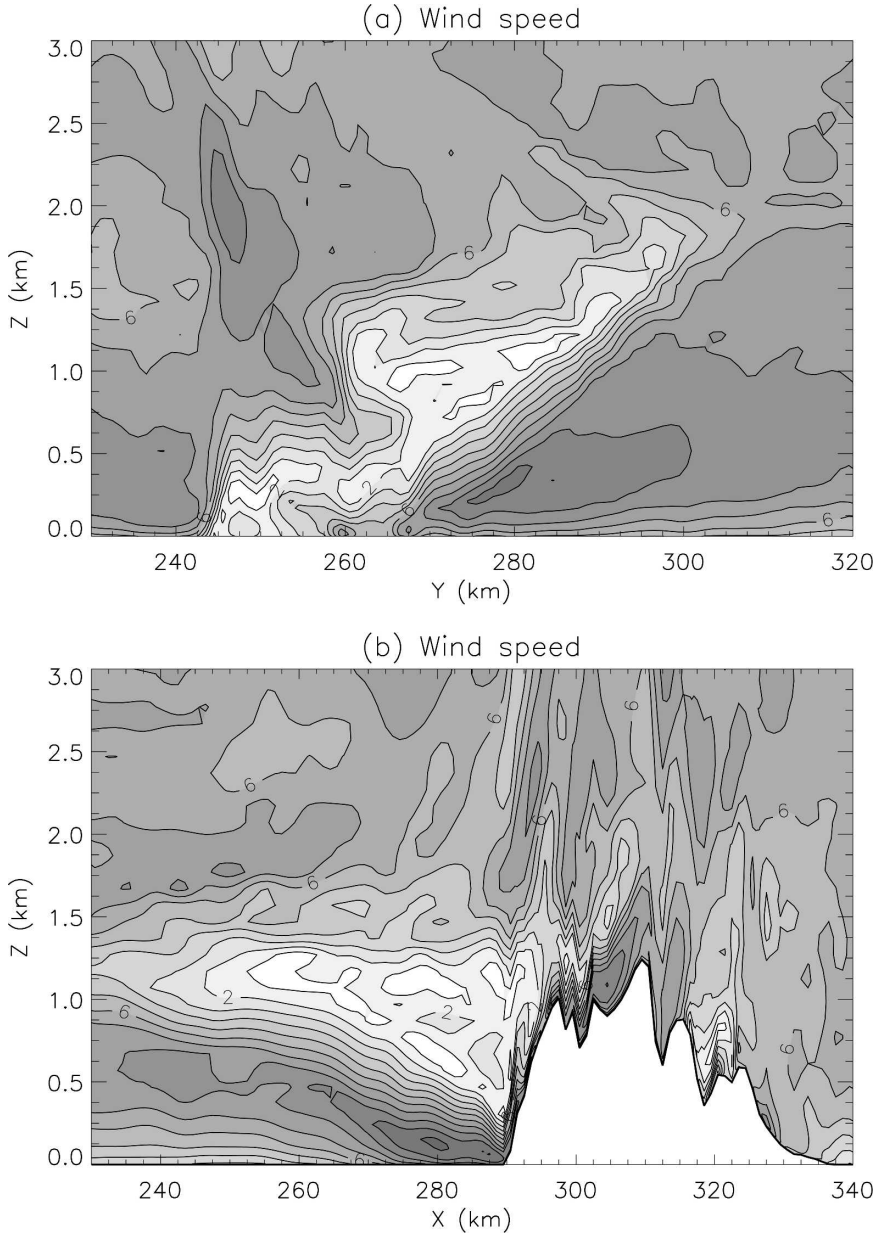

FIG. 6. Cross sections of wind speed from domain 3 of the 1200 UTC 26 Jun simulation. (a) Meridional cross section through $X = 272$ km, and (b) zonal cross section through $Y = 275$ km (see Fig. 5). Wind is contoured at 1 m s^{-1} intervals, and darker shading represents higher speeds.

vertical structure of these shear lines is illustrated in a meridional cross section about 15 km downstream of Kauai (Fig. 6a) and in a zonal cross section through the northern shear line (Fig. 6b). The meridional cross section highlights the tilt of the wake with height. At lower heights, both of the shear lines are farther to the south than at upper levels. It will be shown later that this tilt with height is mostly due to directional shear present in the upstream sounding. The zonal cross section intersects the northern shear line and identifies the location of the low-level jet that forms on the northwestern side of the wake. This jet undercuts the shear line, because of the northward tilt of the wake with height.

Figure 5 also shows regions of parameterized subgrid turbulent kinetic energy (TKE). The subgrid parameterization produces nonzero TKE in regions in which the resolved Richardson number (Ri) is small (<1). In general, the TKE is largest within the shear lines and

the downstream portion of the wake. The next section examines the highest-resolution domain, which explicitly resolves most of the turbulence that is parameterized in this 1-km-grid-spacing domain.

The temporal and spatial variability of the winds within the wake and the uncertainties in the simulation make a detailed direct comparison between the model simulation and the Helios-measured winds intractable. Nevertheless, the modeled winds shown in Fig. 4 do show some consistency with the winds measured along the Helios flight track (Fig. 2). The wind directions measured at the surface, 170 m, and 500 m (Fig. 2) all compare well to those shown in Figs. 4a–c. The only major difference between the simulations and the measured winds occurs near the top of the flight track (~900–1000 m). Yet, in this region the shear line is near to the track, and the flow should be expected to be highly variable in time and space.

As part of our sensitivity studies, the 26 June simulation was also completed without inclusion of surface sensible heat flux. This simulation therefore did not produce flows induced by heating of the land surface, such as a sea-breeze circulation. The structure of the wake, however, was very similar to that shown with heating, and the location and intensity of the shear lines were each very similar. The only notable difference was a slightly weaker onshore flow in the lee of Kauai. The 0000 UTC (1400 LST) 27 June sounding was also used to initialize the model in another sensitivity study. This sounding was very similar to the 1200 UTC 26 June sounding, and the modeled wake structure was qualitatively similar also.

To initialize the model, the Lihue sounding is used to define the background flow conditions. This sounding is released from the southeastern side of Kauai (see Fig. 2) in a region in which the flow direction is influenced by low-level blocking and sea breezes (see Fig. 4). To examine the influence of blocking on the modeled solution, a model sounding from domain 3 at Lihue was compared with the real Lihue sounding. This comparison showed that at this location the flow blocking only affected the model solution in the lowest 100 m, with the wind attaining a slightly stronger northerly component. Simulations with modified low-level wind profiles (not shown) all showed very similar wake structures aloft, with only minor differences in the orientation of the wake at the surface. Given this lack of sensitivity, the use of the Lihue sounding was considered to be acceptable for this study.

c. Turbulent breakdown of the wake

In the previous section, the 1-km-grid-spacing domain illustrated that the wake of Kauai is bounded by shear lines that extend downstream from the island. This simulation produced shear lines that were relatively smooth but contained localized regions of $\mathrm{Ri} < 1$ and relatively large values of parameterized subgrid TKE along their length. In this section, we analyze a higher-resolution domain with 167-m horizontal grid spacing and 50-m vertical grid spacing in an attempt to resolve better the turbulence that is parameterized in the 1-km domain. The location of the 167-m domain (domain 5) is shown in Fig. 2. Domain 5 is centered over the northern shear line, which is the stronger of the two, and is most important for the Helios investigation because of the aircraft's northwestward flight track. This domain is initialized 4 h into the simulations and is integrated forward in time for an additional 2 h.

Horizontal cross sections, at 6-h simulation time and at 1 km MSL, of wind speed, vertical velocity, and the vorticity magnitude are shown in Fig. 7. The wind speed shows the shear lines to have a complicated structure. In the 1-km-grid-spacing simulation considered in section 2b the shear lines were relatively smooth, with the isotachs approximately straight. In this simulation, however, the shear lines have become unstable and have broken down into smaller-scale turbulent eddies. At approximately $(X, Y) = (285, 285)$ km, the wind speed, vertical velocity, and vorticity illustrate a breakdown of the shear line. At this location, the vertical velocity and wind speed exhibit wavelike structures with fronts aligned perpendicular to the mean flow. In the vicinity of this wave, isolated vortices are formed that are advected to the west (downstream) as well as into the region of the wake with relatively slow wind speeds. The vertical velocity exhibits a variety of complicated coherent structures aligned in a variety of directions relative to the background flow.

A zonal cross section of potential temperature through $Y = 285$ km (Fig. 8) shows the vertical extent of the vortices so evident in Fig. 7. This cross section shows waves at the base of the trade wind inversion and also structures resembling classical Kelvin–Helmholtz (K–H) billows at lower levels. The billows are most well defined between approximately 500 and 1000 m MSL surrounding $X = 285$ km. The (vertical and horizontal) wind shear is strong within the shear line, and, coupled with the relatively low static stability below the trade wind inversion, the Richardson number becomes small enough to develop K–H instability. This K–H instability generates turbulent eddies that break down within the shear line, reducing its coherence. These eddies are advected downstream and into the relatively calm wake by the large-scale flow recirculation that characterizes the wake. The K–H billows, wavelike signals in velocity, and resultant eddies possess horizontal scales of

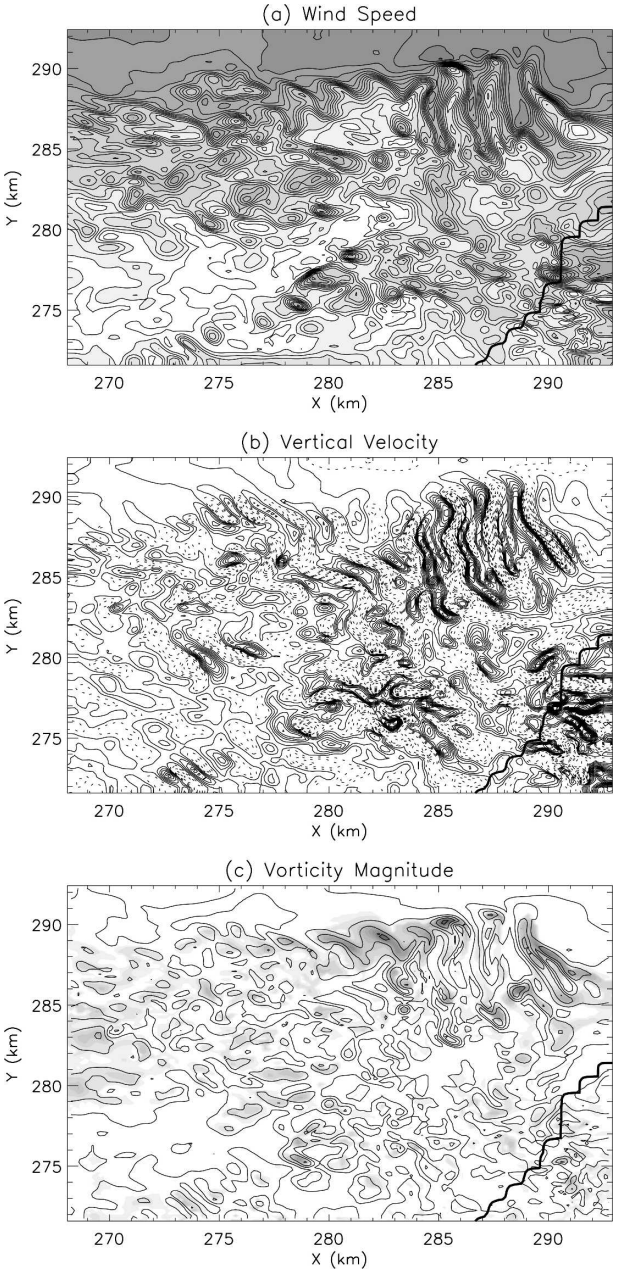

FIG. 7. Horizontal cross sections at 1 km MSL from domain 5 of the 26 Jun 2003 simulation. (a) Wind speed contoured at 0.5 m s^{-1} intervals, and darker shading represents stronger speeds. (b) Vertical velocity contoured at 0.25 m s^{-1} intervals, with negative values dashed. (c) The magnitude of the vorticity vector contoured at 0.01 s^{-1} intervals, with subgrid TKE shaded; the maximum subgrid TKE is approximately 0.65 m^2 s^{-2}.

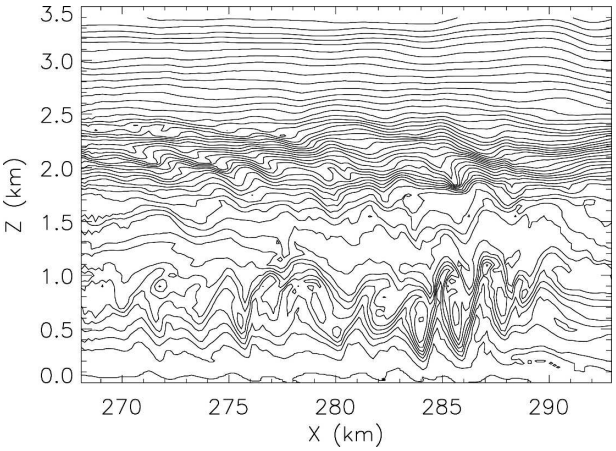

FIG. 8. Zonal cross section of potential temperature through $Y = 285$ km from domain 5 of the 26 Jun 2003 simulation. The contour interval is 0.4 K.

about 2 km and are therefore adequately resolved by the 167-m horizontal grid spacing but not with the 1-km (domain 3) simulations.

Analysis of the resolved vorticity fields (not shown) reveals that the meridional component of the vorticity vector is by far the strongest, being about 3 times the zonal component of vorticity in magnitude. The vertical vorticity is negligible in comparison. The meridional vorticity is dominated by the vertical shear term $\partial u/\partial z$, where u is the zonal wind. In a similar way, the zonal vorticity is dominated by the vertical shear term $\partial v/\partial z$, where v is the meridional wind. Therefore, the zonal component of the vertical wind shear is the strongest term contributing to the vorticity, which is partly due to the vertical tilt of the shear line. The dominance of the meridional vorticity is consistent with flow-perpendicular K–H billows.

The Richardson number is defined as the Brunt–Väisälä frequency squared divided by the total deformation squared. In standard tensor notation,

$$\mathrm{Ri} = \frac{N^2}{\mathrm{Def}^2},$$

where

$$\mathrm{Def}^2 = \frac{1}{2}\sum_i\sum_j D_{ij}^2$$

and

$$D_{ij} = \frac{\partial u_i}{\partial x_j} + \frac{\partial u_j}{\partial x_i} - \frac{2}{3}\,\delta_{ij}\frac{\partial u_k}{\partial x_k},$$

where u_i are the velocity components. Thus, the total deformation includes both horizontal and vertical shear terms that contribute to lowering Ri and encouraging K–H instabilities. In this case, however, the horizontal shear remains weak relative to the vertical shear. For example, Fig. 6a shows that in the northern shear line the vertical (speed) shear is about 15 m s^{-1} km^{-1} and the horizontal speed shear is about 0.7 m s^{-1} km^{-1}. This dominance of the vertical shear is mostly due to the

strong northward tilt of the shear line with height, which has an aspect ratio of about 20:1. If the shear line were oriented exactly vertically, that is, with no tilt, there would be no vertical shear, only horizontal shear. In this case, it is clear that the strength of the vertical shear plays a dominant role in the K–H instability, and the strong vertical shear owes its existence to the northward tilt of the shear line with height.

To examine the robustness of these results to the domain configurations, we conducted two tests. The first test was to rerun the highest-resolution domain in a different location, approximately 10 km to the south (not shown). This domain encompassed the northern shear line (at low levels) and the southern shear line (at upper levels). Both shear lines developed turbulence in a fashion qualitatively similar to that presented here. The second test was to examine results from the next-coarsest domain (domain 4) in a simulation that did not include the 167-m domain (domain 5). This simulation showed that at 500-m horizontal grid spacing the wake was more transient than in domain 3; however, turbulent eddies still did not form. It will be shown in the next section that at 167-m grid spacing the model does in fact resolve a part of the inertial range, allowing turbulence to form.

Therefore, the reduction of the grid spacing from 1 km to 167 m has better resolved the northern shear line. This increased resolution has allowed turbulent eddies to form as a consequence of the breakdown of the shear line through K–H instability. The result is a turbulent transition zone that lacks the coherence of the shear lines seen in the coarser-resolution simulation but still defines the wake boundary.

d. *Characterization of the turbulence within the wake*

The resolved fields within the highest-resolution domain (domain 5) of the 26 June simulation can be analyzed to estimate the turbulence levels within the wake. To do so, values of spatial second-order velocity structure functions were computed from numerical model output in a manner similar to that described in Frehlich and Sharman (2004) to infer eddy dissipation rate. For a homogeneous field the local horizontal spatial statistics of the model output variable $\tilde{q}$ can be computed from second-order structure functions:

$$D_{\tilde{q}}(r, s, z) = \langle [\tilde{q}(x, y, z) - \tilde{q}(x + r, y + s, z)]^2 \rangle, \tag{2.1}$$

where $\langle\,\rangle$ denotes an ensemble average and r and s are separations (or lags). Because the model fields $\tilde{q}$ have been spatially averaged (by numerical smoothing and filtering), the model-derived structure functions are filtered versions of the true structure functions. At shorter lags, the structure functions reflect the smallest scales resolved by the model, but these scales are the most heavily filtered and therefore cannot be used to infer turbulence intensities directly. At larger lags, the structure functions reflect the larger scales in the model, which are not so heavily filtered, and so turbulence-level estimates using the information from the larger lags are more reliable, although even these estimates must be considered to be a lower bound because of some minimal model filtering at the larger scales.

Note that the structure functions provide a spatial average of the turbulence over the analysis domain, and therefore the assumption of homogeneous turbulence over the analysis domain will have a small effect on the interpretation of the turbulence levels; that is, the highest turbulence levels will be larger than the spatially averaged estimate. More information about the spatial variations of the turbulence field is required to quantify the effects of assuming locally homogeneous turbulence [see Frehlich and Sharman (2004) for more details].

Longitudinal and transverse structure functions are computed from model output fields of zonal velocity u and vertical velocity w using Eq. (2.1) for portions of the model grid of interest and are then averaged in the y direction and over three vertical levels, including one model level above and one model level below the level of interest. The values of these global-average structure functions are then plotted as a function of separation index s. We assume that for some intermediate values of s the magnitudes of the longitudinal $D_{\mathrm{LL}}(s)$ and transverse $D_{\mathrm{NN}}(s)$ structure functions will obey the Kolmogorov relations [e.g., Monin and Yaglom 1975, their Eq. (2.17′)]:

$$D_{\mathrm{LL}}(s) = C_K \varepsilon^{2/3} s^{2/3} \quad \text{and} \tag{2.2a}$$

$$D_{\mathrm{NN}}(s) = \frac{4}{3} C_K \varepsilon^{2/3} s^{2/3}, \tag{2.2b}$$

where the turbulence intensity is measured by the eddy dissipation rate ε and $C_K \approx 2$ is the Kolmogorov constant. These relations are valid for separations s much less than the integral length scale L_0. In general, L_0 is not known a priori but can be inferred from plots of $D_{\mathrm{LL}}(s)$ and $D_{\mathrm{NN}}(s)$ as a function of the separation distance s. Note that for $s < L_0$, $D_{\mathrm{LL}}(s)$ and $D_{\mathrm{NN}}(s)$ have an $s^{+2/3}$ slope, and as s approaches L_0 the slope starts to deviate from +2/3 and (ideally) the structure functions become a constant at large separations. As is well known, within the convective boundary layer the length scale for the vertical velocity component is much

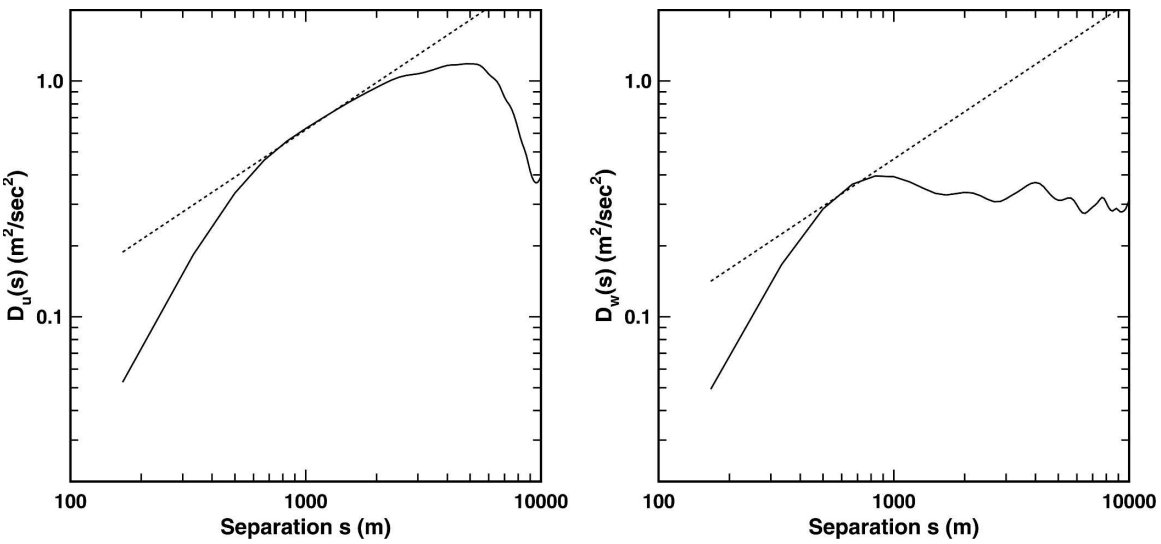

FIG. 9. Structure functions (solid line) derived from model output of domain 5 (167-m grid spacing) for the 26 Jun case at an altitude of 1000 m for (left) zonal velocity u and (right) vertical velocity w. The best-fit Kolmogorov model is also shown (dotted line).

less than the length scale for the horizontal velocity components (see, e.g., Kaimal and Finnigan 1994, chapter 2).

Using these ideas, average turbulence intensities were derived from the 26 June simulation in the northwest quadrant of the resolved wake and at $z = 1000$ m, that is, near the location and altitude of the Helios breakup. Inspection of Fig. 7 shows that at this level the northwest quadrant is downstream of the K–H breakdown region and has the strongest variability away from this region; that is, it represents well-developed turbulence. Figure 9 shows the u (longitudinal) and w (transverse) average structure functions computed from the model (denoted D_u and D_w, respectively) over this region. The u (longitudinal) structure function exhibits a well-defined Kolmogorov scaling region over a wide range from about 600 to 1500 m; that is, L_0 is about 2000 m. Using Eq. (2.2a) and an approximate fit to the inertial range (dotted line), we estimate a lower bound to the turbulence level of $\varepsilon_u^{1/3} = 0.056$. The structure function for the vertical velocity derived from the model does not resolve the Kolmogorov behavior very well because the integral scale L_0 is relatively small (approximately 500 m). The best-fit Kolmogorov level (dotted line) predicts a lower bound to the turbulence level of about $\varepsilon_w^{1/3} = 0.042$, which is not greatly different from the predictions using the longitudinal velocity structure function.

If we assume the small-scale turbulence in the model has a 3D isotropic Kolmogorov description, then $\varepsilon_w^{1/3} \sim \varepsilon_u^{1/3}$ and this level should be maintained down to smaller scales along the dotted line in Fig. 9. However, this neglects the inherent model filtering at small scales demonstrated by the solid line, which is more pronounced for the vertical velocity because of the smaller length scale. Equation (2.2b) implies that the lower bound for the 1-σ vertical velocity difference over the 100-m Helios wingspan is about $[D_w(s = 100 \text{ m})]^{1/2} = [8/3\varepsilon_u^{2/3}(100)^{2/3}]^{1/2} = 0.42 \text{ m s}^{-1}$. The lower bound of the 2-σ vertical velocity difference is therefore about 0.8 m s^{-1}. These values could be used to determine whether it was likely that the Helios encountered aerodynamic loads that exceeded its design capacity. These computations were also performed for other quadrants in the simulation domain (not shown) and produced somewhat lower estimates of turbulence levels.

3. Sensitivity experiments

In section 2, simulations describing the wake of Kauai on 26 June 2003 were presented. The simulations showed that the wake extended approximately 40 km downstream, remained attached to the island (i.e., no vortex shedding), and was bounded by strong shear zones that were intense enough to cause breakdown through K–H instabilities into smaller turbulent eddies that were advected predominantly downstream and, to a lesser extent, into the wake itself. In this section, a number of sensitivity studies are presented to examine the effect of changing upstream flow conditions on the wake structure. A number of simulations were also completed that examined the effect of varying the upstream thermodynamic structure; however, these simulations found little sensitivity to the details of the trade

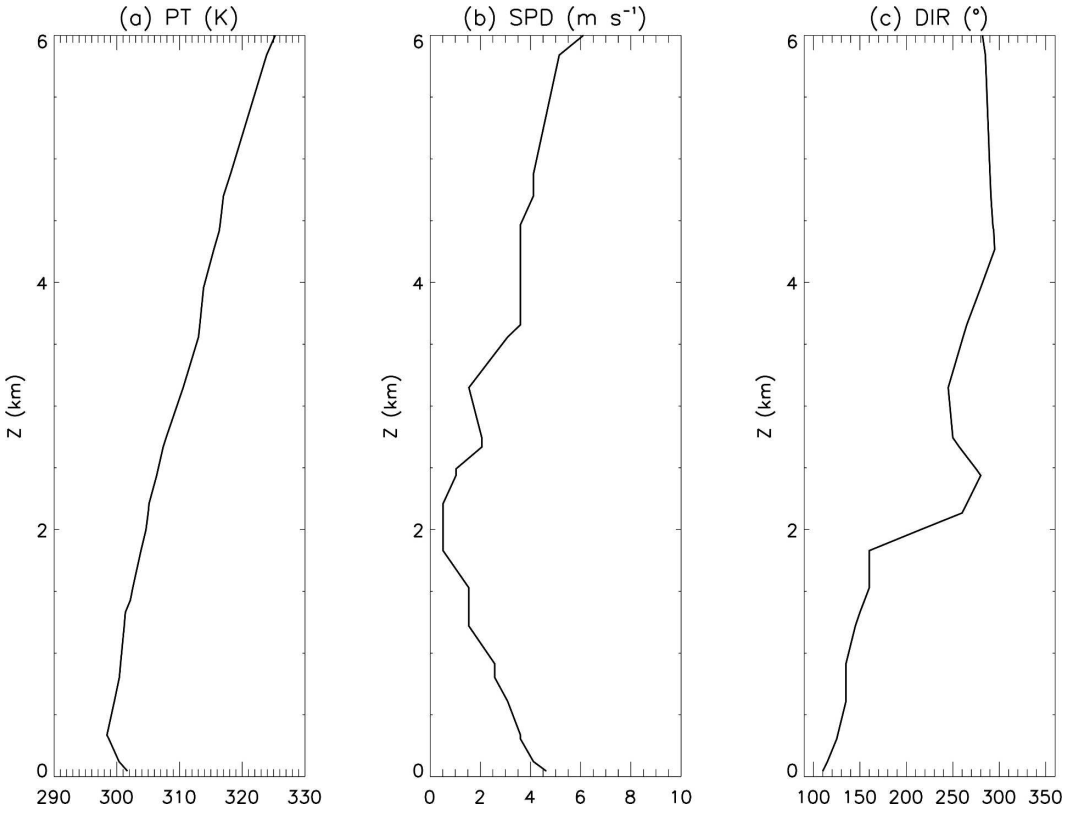

FIG. 10. Profiles of (a) potential temperature, (b) wind speed, and (c) wind direction from the 0000 UTC 7 Jun 2003 PHLI sounding.

wind inversion (i.e., its altitude and strength) when these quantities were varied within reasonable bounds defined by the available observations, and they will therefore not be presented. The sensitivity experiments presented here are not designed to describe the entire parameter space that governs the Kauai wake dynamics; rather, a few cases are chosen to explain a few of the key dependencies of the wake structure on upstream conditions.

a. 7 June 2003 case

On 7 June 2003 the Helios aircraft operated under the same configuration as the 26 June 2003 flight without incident. It was noted by Helios operations that this flight was one of the least turbulent experienced out of nearly a score of flights of this or similar aircraft over several years. This day was examined to determine the differences between the flow conditions on the two days. The 0000 UTC 7 June 2003 Lihue sounding was used to initialize the model in the same way as the 26 June case. This sounding is shown in Fig. 10, and horizontal cross sections of the wind speed at 500 m and 1 km MSL are shown in Fig. 11. The thermodynamic structure sampled by the 6 June sounding is similar to that in the 26 June sounding, except that the trade inversion (or stable layer) is less well defined. The primary difference between the two is the wind profile. The 6 June sounding has much weaker winds of about 3 m s^{-1} below the inversion (as compared with 7 m s^{-1} for the 26 June case). The simulation shows that the wake has a similar shape and orientation to that seen on 26 June; the primary differences are the strength of the shear lines that bound the wake and the depth of the wake. In this case, the low upstream wind speed means that the wind speed difference between the flow within the wake ($\sim$1 m s^{-1}) and outside the wake ($\sim$3 m s^{-1}) is smaller than that seen in the 26 June case. As a consequence, the wind shear is not very strong, and there is less likelihood of turbulent breakdown of the shear lines. The parameterized TKE is also shown in Fig. 11, and its magnitude and extent are much smaller than that seen in Fig. 5. The wake is much shallower in this simulation than in the 26 June case; this difference is consistent with the simulations of Smolarkiewicz and Rotunno (1989), who showed that an increased nondimensional mountain height (or reduced wind speed) could result in a shallower wake.

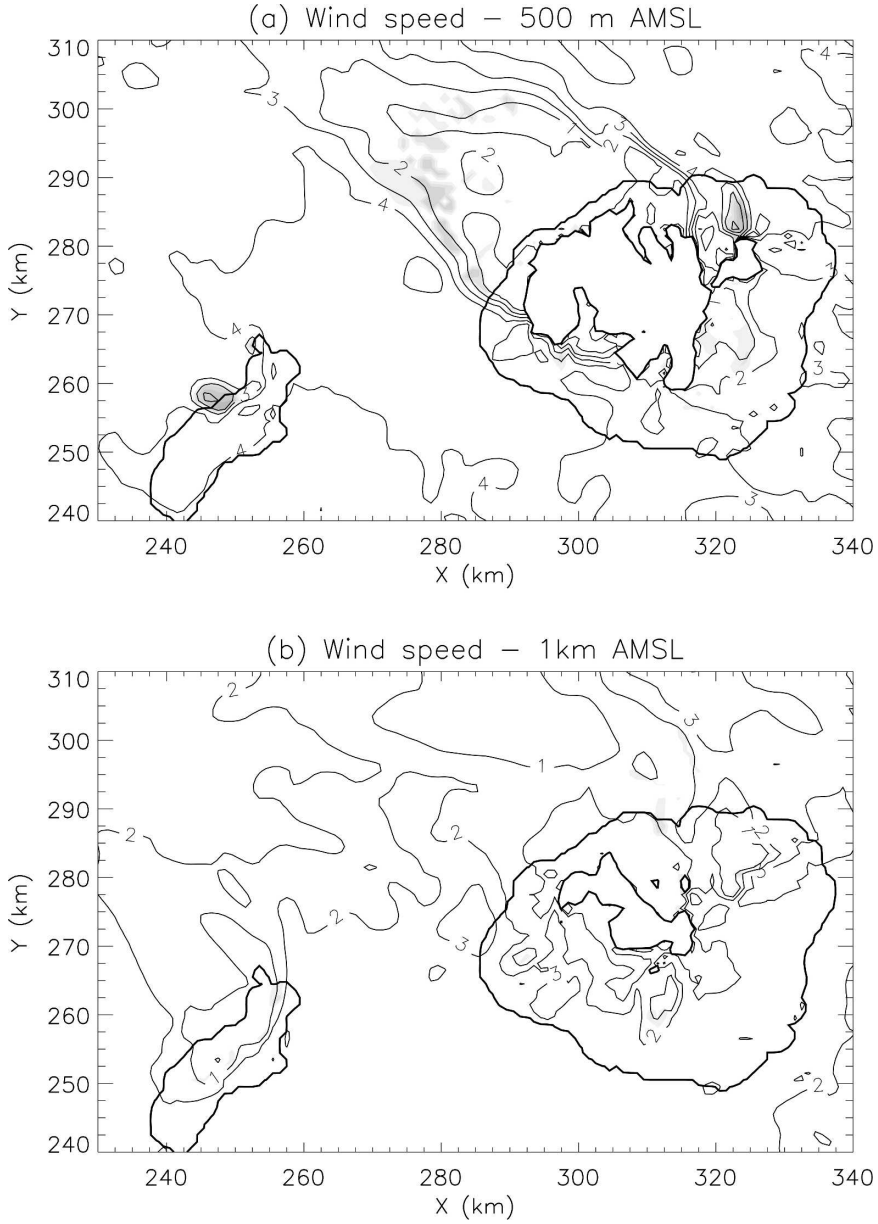

FIG. 11. Horizontal cross section of wind speed at (a) 500 and (b) 1000 m MSL from domain 3 of the 0000 UTC 7 Jun simulation. Wind speed contours have 1 m s^{-1} interval. Also shown is parameterized TKE (shaded); the maximum TKE in (a) is approximately 0.3 m^2 s^{-2}. Note that these figures do not show the entire horizontal extent of domain 3.

b. Sensitivity to wind speed

To examine further the sensitivity of the wake to incident wind speed, two more simulations were completed. Both used the same thermodynamic and wind direction profiles as were used in the 26 June case simulation. In the first case the wind speed at each level was halved, and in the second case the wind speed at each level was doubled. Horizontal cross sections of the wind speed for these two cases are shown in Fig. 12, and a plot from the 26 June case is also shown for comparison. To aid in the comparison, the contour and shading intervals for each plot are scaled according to the wind speed multiplier.

While Figs. 12a and 12b have substantial differences, they show qualitatively similar wakes of similar relative intensity and horizontal extent. The wakes are both bounded by shear lines, except the case with halved wind speed (Fig. 12a) has a much weaker southern shear line. Both the case with reduced wind speed and

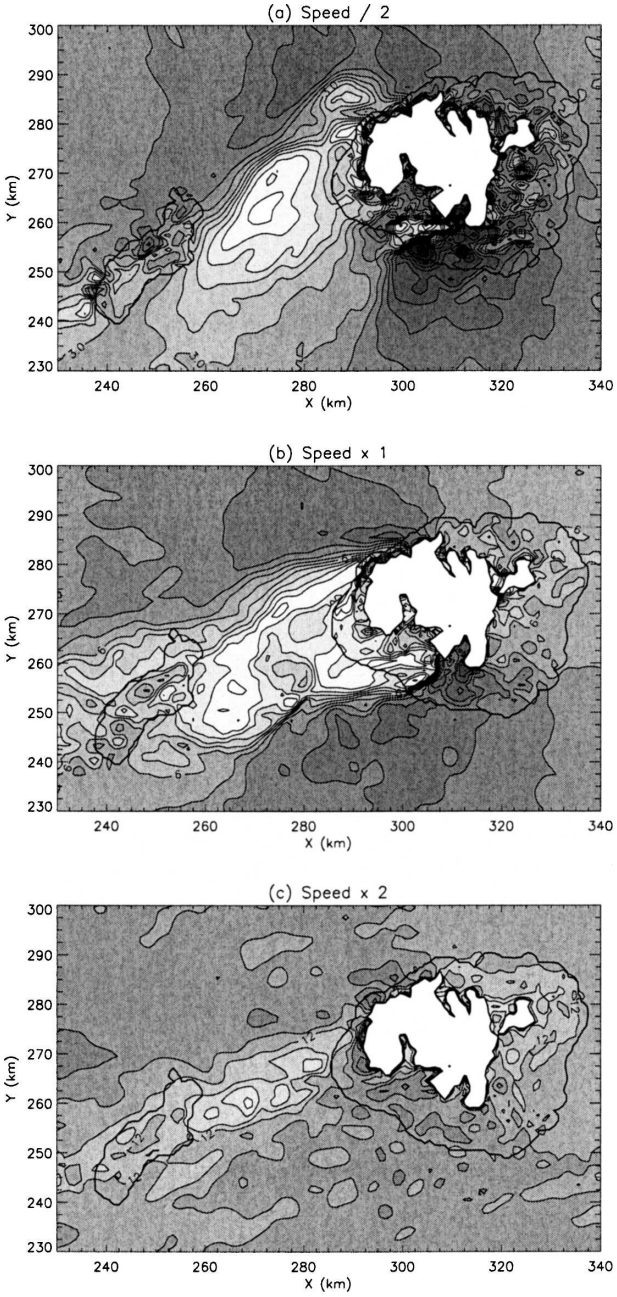

FIG. 12. Horizontal cross sections of wind speed at 500 m MSL for cases in which the wind speed from the 26 Jun 2003 sounding is multiplied by (a) 0.5 ($\hat{h} \sim 3.33$), (b) 1 ($\hat{h} \sim 1.67$), and (c) 2 ($\hat{h} \sim 0.83$). Contour level is 0.5 m s^{-1} in (a), 1 m s^{-1} in (b), and 2 m s^{-1} in (c). Darker shading represents faster wind speeds.

the 26 June case show a substantial wind speed reduction within the wake and evidence of acceleration resulting from blocking on the northern and southern sides of the island. The case with reduced wind speed also has a shallower wake than the 26 June case (not shown) and has much less parameterized TKE than is found in the 26 June case. The case with reduced wind speed has a nondimensional mountain height of about 3.33, as compared with the 26 June case, which has a nondimensional mountain height of about 1.67. The above results are consistent with previous studies that showed that there is no major flow-regime change within this range of values of $\hat{h}$.

However, the increased wind speed simulation in Fig. 12c shows a very different flow structure relative to the previous cases. The flow shows very little evidence of blocking, with little acceleration of the wind at the northern and southern sides of the island. There is some evidence of a weak elongated wake; however, it is much weaker in relation to the 26 June case and the case with reduced wind speed. This case with increased wind speed has $\hat{h} \approx 0.83$; this reduction in nondimensional mountain height has clearly induced a change in flow regime.

The flow-regime change among the three cases is also illustrated by zonal cross sections of potential temperature in Fig. 13. The three cases show that as the nondimensional mountain height decreases from ~3.33 (Fig. 13a) to ~1.67 (Fig. 13b) to ~0.83 (Fig. 13c) the amplitude of the perturbations in potential temperature above the island increases. Figures 13a and 13b show relatively low amplitude gravity waves aloft; Fig. 13c shows large-amplitude gravity waves above the island. This figure clearly shows the change in flow regime from a quasi-blocked flow inducing a wake to a predominantly gravity-wave regime. These results are in qualitative agreement with those of Smolarkiewicz and Rotunno (1989) and other idealized studies.

It is important to note that the above simulations do not isolate the influence of vertical wind shear in defining the structure of the wake. The vertical shear will undoubtedly influence low-level trapping of lee waves through vertical variations in the Scorer parameter and other changes in the downstream structure. The magnitude of the vertical wind shear may generate a large parameter space that certainly warrants investigation but is beyond the scope of this study. Directional shear will be considered briefly in the next section to determine its role in defining the shear line orientation.

c. Wind direction and directional shear

The simulations described earlier show that the lateral wake boundaries, that is, the shear lines, show an orientation that is approximately aligned with the upstream wind direction. To investigate this effect further, two sensitivity simulations are completed.

The first simulation uses the 26 June thermodynamic sounding, with the wind speed set to 7 m s^{-1} and an easterly direction throughout the depth of the sound-

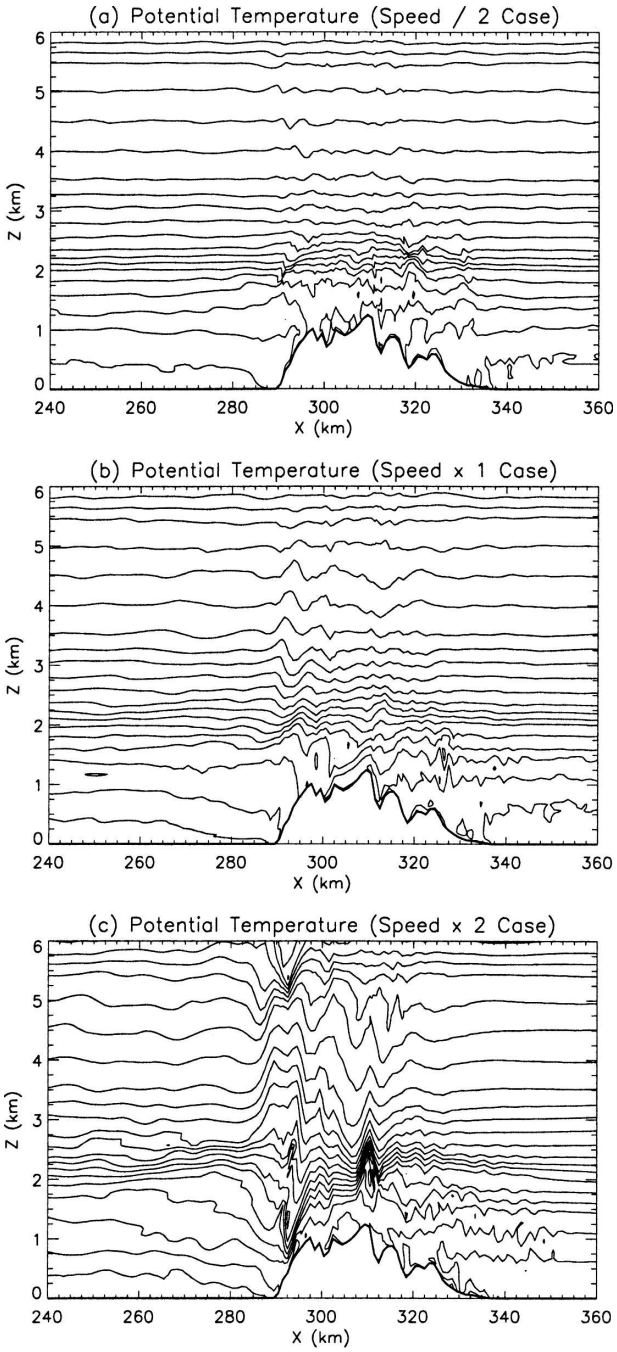

FIG. 13. Zonal cross sections of potential temperature at Y = 275 km for cases in which the wind speed from the 26 Jun 2003 sounding is multiplied by (a) 0.5 ($\hat{h} \sim 3.33$), (b) 1 ($\hat{h} \sim 1.67$), and (c) 2 ($\hat{h} \sim 0.83$). Potential temperature is contoured at 1.5-K intervals, with the outline of the topography also shown.

ing. The results from this simulation are shown in Fig. 14a, using a meridional cross section of the wind speed about 7 km downstream of the island. This figure shows that the shear lines downstream of the island exhibit very little tilt with height; the southern shear line is aligned almost exactly vertically and the northern shear line has only slight northward tilt with height. This wake certainly shows much less systematic tilt than is seen in the 26 June case. The wake, however, is not symmetric, and it contains many detailed structures, probably due to the complicated topography of Kauai. Also, this wake does not extend as far downstream as that in the 26 June case and is less coherent (not shown). This result may be due to the removal of vertical shear in the sounding; this topic is the subject of continuing research. This simulation shows that the removal of directional wind shear from the upstream sounding removes the majority of the cross-stream tilt of the wake with height.

To explore the role of directional shear further, a second simulation is performed. This second simulation retains a constant wind speed of 7 m s^{-1} but uses a wind direction that rotates with height from being southeasterly at the surface to northeasterly at mountaintop, and it remains northeasterly aloft. This wind rotation is more rapid than and is in the opposite sense to that of the 26 June case. Figure 14b shows that downstream of the island the wake has a dramatic tilt toward the south as altitude is increased. As expected, the shear line orientation is from the southeast to northwest at the surface and rotates with the wind to be from the northeast to southwest at the mountaintop (not shown), inducing the tilt seen in Fig. 14b.

These two simulations imply that the directional wind shear in the 26 June sounding is responsible for the change in orientation of the wake boundaries and therefore the vertical tilt of the wake seen in the meridional direction. The orientation of the wake matches the upstream wind direction at that height, which is an intuitive result. This result also implies that any low-level contamination of the upstream sounding resulting from flow blocking should have little effect on the structure of the wake at upper levels. Last, the role of directional shear in creating a meridional tilt in the wake with height is important because the meridional tilt strengthens the vertical shear and plays a key role in generating turbulence within the wake.

4. Summary

In this study a nested nonhydrostatic model has been used to examine the structure of the wake of Kauai on 26 June 2003. The model was configured using up to 5 two-way nested domains; the horizontal grid spacing of these domains varied from 6 km down to 167 m. The majority of the analyses presented used three domains only, focusing on the 1-km-horizontal-grid-spacing do-

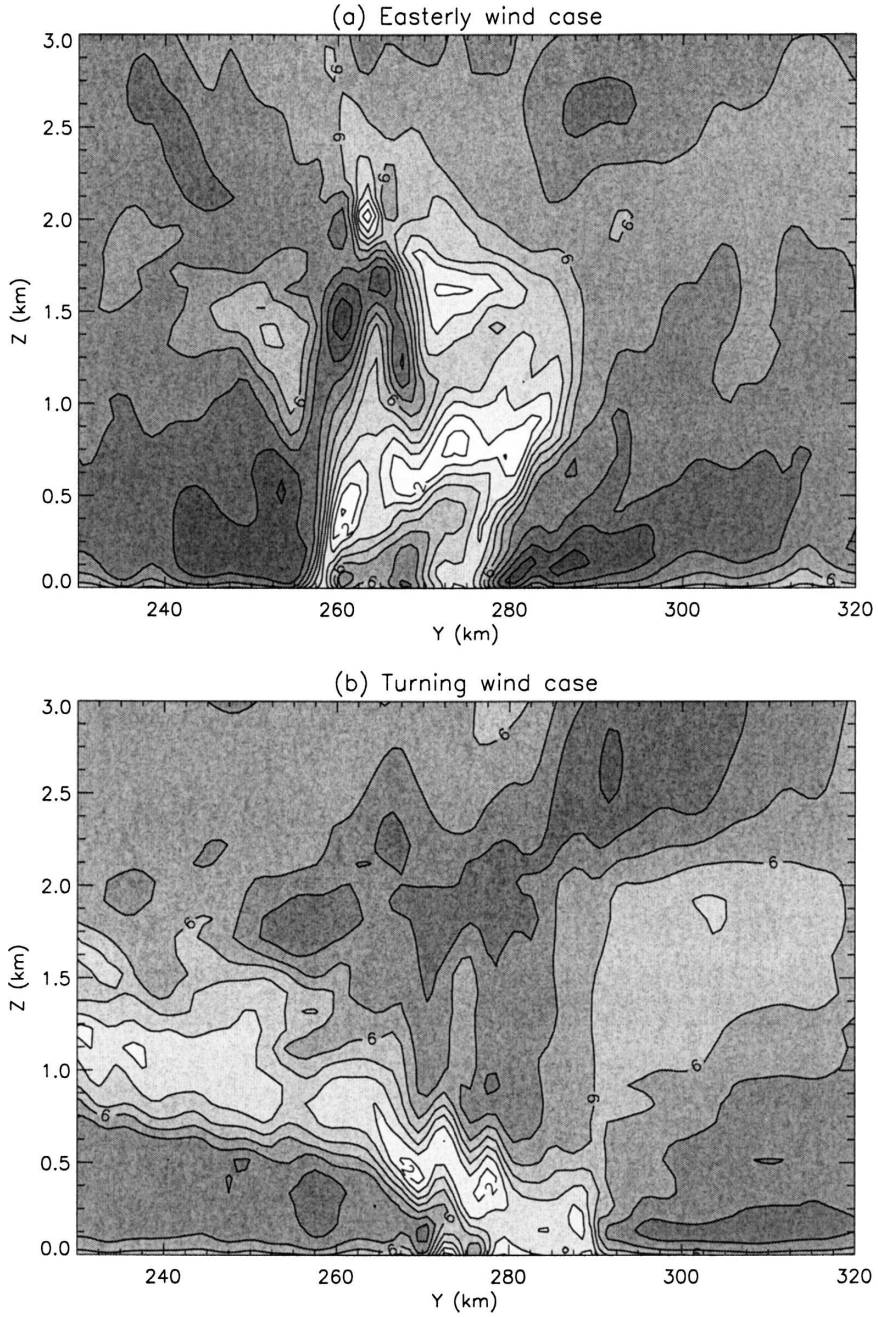

FIG. 14. Meridional cross sections of wind speed contoured at 1 m s^{-1} interval, with darker shading representing faster wind speed: (a) a case with purely easterly wind upstream, with the cross section at $X = 280$ km, and (b) a case in which the wind is from the southeast at the surface and turns to the northeast at mountaintop, with the cross section at $X = 272$ km.

main. The simulations were initialized with a single sounding observed at Lihue, which is located on the southeastern shore of Kauai.

For the 26 June 2003 case, the wind was from the east-northeast and its speed was approximately 7 m s^{-1}. These conditions equated to a low-level upstream non-dimensional mountain height $\hat{h} = Nh/U$ of about 1.67. The simulation produced a well-defined wake extending approximately 40 km downstream from the western shore of Kauai and was bounded by regions with strong vertical and horizontal wind shear—that is, shear lines. The shear lines marked the edges of the wake and in

the horizontal plane were oriented approximately parallel to the upstream wind direction at each respective height. It was subsequently shown that directional shear induced a change in orientation of the wake and produced a pronounced northward tilt of the wake boundaries with height. This tilt caused the vertical wind shear to be about 20 times the horizontal wind shear. In contrast to the observations of the Hawaiian wake by Smith and Grubišić (1993), the northern shear line was the stronger of the two, representing a difference in the asymmetry of the topography in the two islands.

In the 1-km-grid-spacing domain, the shear lines that bounded Kauai's wake had strong enough vertical shear that the local Ri was reduced to values <1 and therefore produced regions of large parameterized subgrid TKE. A higher-resolution simulation resolved one of the shear lines with 167-m horizontal grid spacing, which was able to resolve at least some of the turbulence within the shear line, which formed as a result of Kelvin–Helmholtz instability. The instability formed flow-perpendicular billows and formed turbulent eddies that were advected downstream and into the relatively calm wake flow, leading to a fully turbulent wake. Thus, the interior of the wake is highly unsteady at the smallest resolved scales in the simulations, although the mean wake boundaries show little fluctuation. The K–H breakdown process was not observed to be periodic, and the classical von Kármán vortex street was not observed. This result is consistent with the findings of Etling (1989) and Kang et al. (1998), who showed that a condition necessary for vortex street formation was that the upstream nondimensional mountain height be large, $\hat{h} > 2.5$ and $\hat{h} > 4.5$, respectively. The breakdown of the shear lines into turbulence may have been a factor in the Helios mishap on this day, but because of both uncertainties in the simulations and the temporal and spatial variability of the turbulence, this is impossible to ascertain.

Quantitative estimates of the small-scale turbulence statistics were produced using a technique that accounts for the inherent filtering of the model fields at small scales. More accurate estimates of these statistics are possible, especially for the vertical velocity fields (where the length scales are smaller), using more rigorous corrections for the model's spatial filter (see Frehlich and Sharman 2004). This topic is the subject of continuing research.

Sensitivity studies showed that reducing the wind speed to one-half of that observed on 26 June produced a similar wake, both in terms of its lateral extent and relative strength. However, the case with reduced wind speed produced much less parameterized turbulence within the shear lines than was seen on 26 June. Increasing the wind speed to 2 times that on 26 June produced a very different flow regime. The flow did not show much evidence of blocking, nor was there a well-defined wake. These results imply that a flow-regime change occurs between a nondimensional mountain height of 1.67 (the 26 June case) and 0.83 (the increased wind speed case). This result is consistent with previous experimental and idealized studies.

This study documented the wake of Kauai and briefly examined the sensitivity of some key components of Kauai's wake to upstream conditions. The modeled wake of Kauai is strongly affected by complexities in the topography and the real upstream conditions used, but some features of the wake compared well to previous idealized studies, and therefore some of these results probably apply more generally. This study also documented the formation of turbulence in the shear lines that define the boundaries of Kauai's wake. Further studies of turbulence generation in mountain/island wakes are planned for the future.

Acknowledgments. This work was funded in part by the NASA Helios Mishap Review Board. Special thanks are given to John Madura for his support of this work. This study has benefited from the authors' interactions with Craig Epifanio, Jack Ehernberger, John Porter, and Duane Stevens. We also thank two anonymous reviewers for their comments that helped to improve the manuscript.

REFERENCES

Baines, P. G., 1995: *Topographic Effects in Stratified Flows.* Cambridge University Press, 482 pp.

Brighton, P. W. M., 1978: Strongly stratified flow past three-dimensional obstacles. *Quart. J. Roy. Meteor. Soc.,* **104,** 289–307.

Burk, S. D., T. Haack, L. T. Rogers, and L. J. Wagner, 2003: Island wake dynamics and wake influence on the evaporation duct and radar propagation. *J. Appl. Meteor.,* **42,** 349–367.

Castro, I. P., W. H. Snyder, and G. L. Marsh, 1983: Stratified flow over three-dimensional ridges. *J. Fluid Mech.,* **135,** 261–282.

Chopra, K. P., and L. F. Hubert, 1965: Mesoscale eddies in wake of islands. *J. Atmos. Sci.,* **22,** 652–657.

Clark, T. L., 1977: A small-scale dynamic model using a terrain-following coordinate transformation. *J. Comput. Phys.,* **24,** 186–215.

——, and R. D. Farley, 1984: Severe downslope windstorm calculations in two and three spatial dimensions using anelastic interactive grid nesting: A possible mechanism for gustiness. *J. Atmos. Sci.,* **41,** 329–350.

——, and W. D. Hall, 1996: The design of smooth, conservative vertical grids for interactive grid nesting with stretching. *J. Appl. Meteor.,* **35,** 1040–1046.

——, T. Keller, J. Coen, P. Neilley, H.-M. Hsu, and W. D. Hall, 1997: Terrain-induced turbulence over Lantau Island: 7 June

1994 Tropical Storm Russ case study. *J. Atmos. Sci.,* **54,** 1795–1814.

Ehernberger, L. J., C. Donohue, and E. H. Teets Jr., 2004: A review of solar-powered aircraft flight activity at the Pacific missile range test facility, Kauai, Hawaii. *Extended Abstracts, 11th Conf. on Aviation, Range, and Aerospace Meteorology*, Hyannis, MA, Amer. Meteor. Soc., CD-ROM, P8.3.

Epifanio, C. C., and D. R. Durran, 2002: Lee-vortex formation in free-slip stratified flow over ridges. Part I: Comparison of weakly nonlinear inviscid theory and fully nonlinear viscous simulations. *J. Atmos. Sci.,* **59,** 1153–1165.

——, and R. Rotunno, 2005: The dynamics of orographic wake formation in flows with upstream blocking. *J. Atmos. Sci.,* **62,** 3127–3150.

Etling, D., 1989: On atmospheric vortex streets in the wake of large islands. *Meteor. Atmos. Phys.,* **41,** 157–164.

Frehlich, R., and R. Sharman, 2004: Estimates of turbulence from numerical weather prediction model output with applications to turbulence diagnosis and data assimilation. *Mon. Wea. Rev.,* **132,** 2308–2324.

Hafner, J., and S.-P. Xie, 2003: Far-field simulation of the Hawaiian wake: Sea surface temperature and orographic effects. *J. Atmos. Sci.,* **60,** 3021–3032.

Hawthorne, W. R., and M. E. Martin, 1955: The effect of density gradient and shear on the flow over a hemisphere. *Proc. Roy. Soc. London A,* **232,** 184–195.

Hubert, L. F., and A. F. Krueger, 1962: Satellite pictures of mesoscale eddies. *Mon. Wea. Rev.,* **90,** 457–463.

Hunt, J. C. R., and W. H. Snyder, 1980: Experiments in stably and neutrally stratified flow over a model three-dimensional hill. *J. Fluid Mech.,* **96,** 671–704.

Kaimal, J. C., and J. J. Finnigan, 1994: *Atmospheric Boundary Layer Flows—Their Structure and Measurement*. Oxford University Press, 289 pp.

Kang, S.-D., F. Kimura, and S. Takakashi, 1998: A numerical study on the Kármán vortex generated by divergence of momentum flux in flow past an isolated mountain. *J. Meteor. Soc. Japan,* **76,** 925–935.

Lavoie, R. L., 1967: Air motions over the windward coast of the island of Hawaii. *Tellus,* **19,** 354–358.

Leopold, L. B., 1949: The interaction of trade wind and sea breeze, Hawaii. *J. Meteor.,* **6,** 312–320.

Monin, A. S., and A. M. Yaglom, 1975: *Statistical Fluid Mechanics: Mechanics of Turbulence.* Vol. 2. MIT Press, 874 pp.

Rasmussen, R. M., P. Smolarkiewicz, and J. Warner, 1989: On the dynamics of Hawaiian cloud bands: Comparison of model results with observations and island climatology. *J. Atmos. Sci.,* **46,** 1589–1608.

Smith, R. B., and V. Grubišić, 1993: Aerial observations of Hawaii's wake. *J. Atmos. Sci.,* **50,** 3728–3750.

——, A. C. Gleason, P. A. Gluhosky, and V. Grubišić, 1997: The wake of St. Vincent. *J. Atmos. Sci.,* **54,** 606–623.

Smolarkiewicz, P. K., and R. Rotunno, 1989: Low Froude number flow past three-dimensional obstacles. Part I: Baroclinically generated lee vortices. *J. Atmos. Sci.,* **46,** 1154–1164.

——, R. M. Rasmussen, and T. L. Clark, 1988: On the dynamics of Hawaiian cloud bands: Island forcing. *J. Atmos. Sci.,* **45,** 1872–1905.

Teets, E. H., Jr., C. J. Donohue, and P. T. Wright, 2002: Meteorological support of the Helios work record high altitude flight to 96,863 feet. NASA Tech. Memo. NASA/TM-2002-210727, 17 pp.

Vosper, S. B., 2000: Three-dimensional numerical simulations of strongly stratified flow past conical orography. *J. Atmos. Sci.,* **57,** 3716–3739.

Xie, S.-H., W. T. Liu, Q. Liu, and M. Nonaka, 2001: Far-reaching effects of the Hawaiian Islands on the Pacific ocean–atmosphere system. *Science,* **292,** 2057–2060.